Chlamydomonas γ-tubulin mutations reveal a critical role for γ-TuRC in maintaining the stability of centriolar microtubules

Running title: **γ-TuRC's Role in Centriolar Triplet Stability**

Yuki Nakazawa[1,2*], Naoto Kubota[3], Mao Horii[4], Akira Noga[1,4], Yoshikazu Koike[3], Hiroko Kawai-Toyooka[1], Hideo Dohra[5,6], Katsushi Yamaguchi[7], Shuji Shigenobu[7], Ken-ichi Wakabayashi[8], and Masafumi Hirono[1,3]

[1]Department of Frontier Bioscience, Hosei University, Tokyo, 184-8584, Japan
[2]Science and Technology Group, Okinawa Institute of Science and Technology Graduate University, Okinawa, 904-2245, Japan
[3]Graduate School of Science and Engineering, Hosei University, Koganei, Tokyo, Japan
[4]Department of Biological Science, Graduate School of Science, University of Tokyo, Tokyo, 113-0033, Japan
[5]Research Institute of Green Science and Technology, Shizuoka University, Shizuoka, 422-8529, Japan.
[6]Shizuoka Instrumental Analysis Center, Shizuoka University, Shizuoka, 426-8668, Japan
[7]Trans-Scale Biology Center, National Institute for Basic Biology, Aichi, 444-8585, Japan
[8]Department of Industrial Life Sciences, Faculty of Life Sciences, Kyoto Sangyo University, Kyoto, 603-8555, Japan

*Corresponding author
E-mail: yuki.nakazawa@oist.jp

Keywords: Centriole, Triplet microtubule, γ-tubulin, γ-TuRC, *Chlamydomonas*

Abstract

The centriolar triplet microtubule consists of an A-tubule with 13 protofilaments, and B- and C-tubules, each with 10 protofilaments. Although the formation of the triplets has been shown to require γ-tubulin, its specific role in the formation of each tubule remains elusive. We isolated two novel *Chlamydomonas reinhardtii* mutants, *bld13-1* and *bld13-2*, each expressing γ-tubulin with a single amino-acid substitution (T292I or E89D). Similar to known centriole-deficient mutants, both mutants exhibited defects in ciliary assembly, nuclear number, as well as the number and orientation of cytoplasmic microtubules. Genetic analyses of the mutants, along with the expression of the mutant γ-tubulins in the wild-type cells, suggested that both mutants exert dominant-negative effects over wild-type γ-tubulin. Interestingly, although the centrioles in these mutants retained the typical nine triplet structure, their triplets frequently lacked several protofilaments in specific regions of the A- and C-tubules. The protofilament loss occurs more frequently in the proximal region of the centriole. These structural defects suggest a critical role for γ-tubulin in maintaining the stability of the A- and C-tubules of centriolar triplets.

Summary statement

Novel *Chlamydomonas* γ-tubulin mutations cause a partial loss of protofilaments in centriolar microtubules, indicating a critical role of γ-tubulin in structural stabilization of triplet microtubules.

Introduction

Triplet microtubules are a specialized type of microtubule found exclusively in centrioles, structures with 9-fold symmetry that serve as the core of the centrosome and the basal bodies of cilia (flagella). Each triplet consists of an A-tubule, composed of 13

60 protofilaments arranged in a circle, and B- and C-tubules, each composed of 10
61 protofilaments arranged in an arc. When centrioles function as basal bodies, the outer
62 doublet microtubules of the axoneme extend from the A- and B-tubules (Wang and
63 Stearns, 2017; Osinka et al., 2019; Le Guennec et al., 2021). The unique structure of the
64 centriolar triplet microtubules is highly conserved across eukaryotic organisms, yet its
65 assembly mechanism remains poorly understood (Azimzadeh and Marshall, 2010; Wang
66 and Stearns, 2017; Guichard et al., 2023).

67 Similar to the assembly of cytoplasmic microtubules, the triplet assembly likely
68 involves the γ-tubulin ring complex (γ-TuRC) (Guichard et al., 2010; Schweizer and
69 Lüders, 2021; Mukhopadhyay et al., 2026), a major nucleator of tubulin polymerization
70 (Oakley et al., 2015; Wu and Akhmanova, 2017). It is composed of 14 γ-tubulin
71 molecules arranged in an incomplete ring, along with GCP2~6, MZT1, and other
72 proteins. This structure suggests that it serves as a template for microtubule nucleation,
73 positioning each γ-tubulin at the minus end of a protofilament during nucleation (Liu et
74 al., 2021; Thawani and Petry, 2021; Zupa et al., 2021; Sulimenko et al., 2022). In animal
75 cells, numerous γ-TuRCs within the pericentriolar materials (PCM) of the centrosome
76 nucleate cytoplasmic microtubules, enabling the centrosome to function as the
77 microtubule-organizing center (MTOC) (Oakley et al., 2015; Wu and Akhmanova, 2017).

78 In fact, the γ-tubulin or γ-TuRC has been reported to be essential for centriole
79 formation in many organisms (Ruiz et al., 1999; Shang et al., 2002; Dammermann et al.,
80 2004; Gogendeau et al., 2011; Bahtz et al., 2012; Cota et al., 2017). By analogy to its role
81 in cytoplasmic microtubule assembly, the γ-TuRC is thought to function in the
82 nucleation of centriolar triplet microtubules as well. Supporting this hypothesis, cryo-
83 electron microscopy of isolated human centrosomes revealed a conical structure, likely
84 a γ-TuRC, capping the proximal end of the A-tubule in the immature centriole (Guichard
85 et al., 2010). However, the γ-TuRC's nucleation activity for centriolar microtubules has

86 not been directly demonstrated, and its contribution to triplet microtubule assembly
87 and/or maintenance, particularly of the B- and C-tubules, remains unclear.
88 Besides its prominent localization to the PCM, γ-TuRC is also found in various
89 centriolar sites: in the proximal region of the triplet microtubule wall, on the outer and
90 inner (luminal) surfaces of the microtubule wall, and on the distal appendages (Silflow
91 et al., 1999; Schweizer and Lüders, 2021; Kalbfuss and Gönczy, 2023; Laporte et al.,
92 2024). While the specific function of γ-TuRC at each site is unclear, a recent study in
93 human cells showed that the depletion of proteins that localize γ-TuRCs to the inner
94 surfaces of the centriole microtubules destabilizes the centrioles and impairs ciliary
95 assembly (Schweizer et al., 2021). This suggests that the γ-TuRCs within the centriole
96 lumen play a crucial role in maintaining centriole structural integrity.
97 In this study, we isolated two novel *Chlamydomonas reinhardtii* strains carrying
98 missense mutations in the single copy γ-tubulin gene, which appear to exert dominant-
99 negative effects. These are the first viable mutants of the γ-tubulin gene identified in
100 *Chlamydomonas reinhardtii*. Similar to previously reported centriole-deficient mutants,
101 these mutants exhibited defects in ciliary assembly. Intriguingly, their centrioles
102 frequently lacked some of the protofilaments in the A- and C-tubules of triplet
103 microtubules. These phenotypes and the predicted positions of the mutations in the γ-
104 tubulin molecule support the idea that γ-tubulin functions as a γ-TuRC component to
105 stabilize triplet microtubules.
106
107 **Results**
108 **Novel γ-tubulin mutants of *Chlamydomonas***
109 We isolated two independent *Chlamydomonas* strains that showed defects in ciliary
110 assembly and nuclear segregation, which are phenotypes characteristic of known
111 centriole-deficient mutants (Fig. 1 A, B; Table 1) (Ehler et al., 1995; Dutcher and

112 Trabuco, 1998; Matsuura et al., 2004; Hiraki et al., 2007; Nakazawa et al., 2007). As
113 genetic analyses mapped these mutations to the same locus on Linkage Group VI
114 (Chromosome 6), we named the mutants *bld13-1* and *bld13-2* (Fig. 1C). Further linkage
115 analyses showed that the causal mutations exhibited no recombination with a genetic
116 marker designed within the γ-tubulin gene; among 188 progenies examined, no
117 recombinants were detected. Whole genome sequencing of *bld13-1*, and PCR-based
118 sequencing of the *bld13-2* γ-tubulin gene identified point mutations that cause single
119 amino-acid substitutions (*bld13-1*, T292I; *bld13-2*, E89D) in the γ-tubulin gene, a single-
120 copy gene in *Chlamydomonas* (Fig. 1D). The original amino acids at these mutation sites
121 are widely conserved among organisms including single-cell organisms and humans
122 (Fig. 1D). To infer possible effects of these mutations on the γ-tubulin structure, we
123 compared AlphaFold2-predicted models of the *bld13-1* and *bld13-2* γ-tubulins with that
124 of the wild type (Fig. S1A) (Jumper et al., 2021). The models suggest no predominant
125 changes in the molecular conformation, except for a slight change in a small region on
126 the molecular surface of *bld13-1* γ-tubulin.
127 To computationally assess their functional impact, AlphaMissense was applied
128 to human γ-tubulin (UniProt ID P23258) (Cheng et al., 2023). The equivalent E89D and
129 T288I (corresponding to *Chlamydomonas* E89D and T292I, respectively) substitutions
130 were both classified as 'likely pathogenic' (scores: 0.9508 and 0.9956, respectively).
131

132 **The *bld13-1* and *bld13-2* mutations are consistent with a dominant-negative**
133 **mechanism**

134 The defective phenotypes of the *bld13* mutants were not rescued by expression of a
135 hemagglutinin (HA)-tagged γ-tubulin gene (γ-tub(WT)-HA). In addition, expression in
136 wild-type cells of an HA-tagged γ-tubulin gene carrying either the *bld13-1* or *bld13-2*
137 mutation (WT::γ-tub(T292I)-HA or WT::γ-tub(E89D)-HA), driven by the endogenous

138 promoter, caused defects in ciliary assembly similar to those observed in the mutants
139 (Fig. 2 A, B). Together, these results suggest that the mutant γ-tubulins may interfere
140 with wild-type γ-tubulin function, consistent with a dominant-negative effect. To test
141 this possibility under equal gene dosage of wild-type and mutant alleles, we produced
142 diploid strains by crossing the wild type with *bld13-1* or *bld13-2* (WT/*bld13-1*,
143 WT/*bld13-2*), and counted the percentage of cells with no or only one cilium in the two
144 heterozygous strains as well as in the homozygous diploid strain (*bld13-1*/*bld13-2*). The
145 percentages were significantly higher in the heterozygous or homozygous diploid
146 strains carrying the *bld13* mutation than in the wild-type diploid strain (WT/WT) (Fig.
147 2C). These results support the interpretation that the *bld13-1* and *bld13-2* mutations
148 interfere with wild-type γ-tubulin function in a dominant-negative manner.
149

150 **γ-Tubulin localizes to centrioles and their surrounding regions independently**
151 **of *bld13* mutations**

152 In the interphase *Chlamydomonas* cell, two mature centrioles (basal bodies) and two
153 immature centrioles (probasal bodies) are present at the base of the two cilia, forming
154 an organizing center for four stable rootlet microtubule bundles and non-rootlet
155 cytoplasmic microtubules (Fig. 3A; Holmes and Dutcher, 1989). A positional marker for
156 centrioles, SAS-6 localizes to the proximal ends of both mature and immature centrioles
157 and is therefore observed as four discrete fluorescent spots.

158 In wild-type and *bld13* cells expressing HA-tagged wild-type γ-tubulin (Fig. 3B;
159 WT::γ-tub(WT)-HA, *bld13-1*::γ-tub(WT)-HA, and *bld13-2*::γ-tub(WT)-HA), HA signals
160 were detected in regions adjacent to the four centrioles, which are marked by SAS-6
161 fluorescence. Most HA signals were observed as punctate fluorescence in the
162 pericentriolar region, together with diffuse fluorescence distributed throughout this

163 region. Some SAS-6 fluorescent spots overlapped with punctate HA signals, whereas the
164 remaining SAS-6 spots overlapped with the diffuse HA fluorescence.
165 In wild-type cells expressing HA-tagged mutant γ-tubulin (Fig. 3B; WT::γ-
166 tub(T292I)-HA and WT::γ-tub(E89D)-HA), the overall HA localization patterns were
167 essentially indistinguishable from those observed in the cells expressing HA-tagged
168 wild-type γ-tubulin. In all cases, HA signals were detected in association with SAS-6–
169 identified centrioles, together with prominent punctate or diffuse signals in the
170 surrounding regions.
171 These observations indicate that γ-tubulin–HA signals, although not always
172 strongly concentrated, overlap with both mature and immature centrioles, particularly
173 in their pericentriolar regions. Apparently, the *bld13-1* and *bld13-2* mutations do not
174 grossly alter the subcellular localization pattern of HA-tagged γ-tubulin.
175
176 **Cytoplasmic microtubule organization is aberrant in *bld13* cells**
177 In mammalian cells, γ-tubulin localizes to the pericentriolar material (PCM) of the
178 centrosome and functions in the nucleation and organization of cytoplasmic
179 microtubules (Oakley et al., 2015; Wu and Akhmanova, 2017). In *Chlamydomonas* cells,
180 although a distinct PCM has not been observed, functional analogs of PCMs are most
181 likely attached to the centrioles and serve as the site where γ-tubulin functions, as
182 rootlet and non-rootlet cytoplasmic microtubules extend from the proximity of the
183 centrioles (Fig. 3A, Holmes and Dutcher, 1989). To evaluate the effects of the *bld13*
184 mutations on the intracellular microtubule-organization, we performed
185 immunofluorescence microscopy using two kinds of tubulin antibodies. One was an
186 anti–acetylated tubulin antibody, which primarily recognizes axonemal and rootlet
187 microtubules (Fig. 4A), and the other was an anti–α-tubulin antibody, which recognizes
188 both rootlet microtubules and non-rootlet cytoplasmic microtubules (Fig. 4B).

189 When cells were stained with the anti–acetylated α-tubulin antibody, ~60% of
190 wild-type cells exhibited a typical cruciform rootlet arrangement of four microtubule
191 bundles, consistent with the canonical rootlet organization (Fig. 4A). In the remaining
192 ~40% of wild-type cells, five or more acetylated microtubule structures were observed,
193 but it was not possible to definitely identify these microtubules as rootlets. In contrast,
194 the proportion of cells with five or more acetylated microtubules were significantly
195 increased in the mutants, reaching 75% in *bld13-1* and 55% in *bld13-2*. Notably, a subset
196 of mutant cells displayed cage-like cytoplasmic microtubules that did not originate from
197 an obvious organizing center; such cells were observed at frequencies of 3.4% in *bld13-1*
198 and 2.4% in *bld13-2*, but were never observed in the wild type.
199 Staining with the anti–α-tubulin antibody allowed visualization of non-rootlet
200 cytoplasmic microtubules in addition to rootlet microtubules (Fig. 4B). With this
201 antibody, even wild-type cells frequently exhibited five or more microtubules, making
202 the distinction between wild-type and mutant cells less pronounced than with anti–
203 acetylated α-tubulin staining. However, in both *bld13* mutant strains, but not in wild
204 type, cells exhibiting cage-like microtubule arrays were again detected. In these cells,
205 neither acetylated nor non-acetylated microtubules appeared to originate from a
206 discrete microtubule-organizing center.
207 Taken together, these observations indicate that the *bld13-1* and *bld13-2* γ-
208 tubulins are likely to have some defects in organizing microtubules in *Chlamydomonas*
209 cell bodies.
210
211 **Centriolar triplet microtubules frequently lack protofilaments in *bld13***
212 The phenotypes of *bld13* mutants, namely, defective in ciliary assembly, nuclear
213 segregation, and rootlet microtubule organization, are shared by various
214 *Chlamydomonas* mutants having structural defects in the centriole (Ehler et al., 1995;

215 Dutcher and Trabuco, 1998; Matsuura et al., 2004; Hiraki et al., 2007; Nakazawa et al.,
216 2007). Therefore, we examined the centriole structure in *bld13* cells by thin-section
217 electron microscopy. Longitudinal images of *bld13-1* and *bld13-2* centrioles appeared
218 normal (Fig. 5A), although some of those centrioles did not attach axonemes and
219 therefore apparently failed to nucleate ciliary growth. Strikingly, however, obvious
220 defects were observed in cross-sectional images of centrioles in both mutants: some
221 triplet microtubules partially lacked protofilaments (Fig. 5B). In most cases, two to
222 seven adjacent protofilaments were lost from particular positions in the A- and C-
223 tubules, but not in the B-tubules. These abnormalities were never observed in wild-type
224 centrioles (Table 2). To evaluate the cross-sectional positions in the *bld13* centrioles
225 where protofilament loss frequently occurs, the cross-sectional images of the A- or C-
226 tubules were divided into 6 or 12 sectors, and the occurrence of missing protofilaments
227 was scored in each sector. The results showed that the protofilament loss frequently
228 occurred in the sectors that contain protofilaments No. A1-A6 of the A-tubule and No.
229 C1- C7 of the C-tubule in both *bld13-1* and *bld13-2* (the numbering is after Linck and
230 Stephens, 2007 and Li et al., 2019). These data indicate that protofilament loss occurred
231 non-randomly, with a significantly biased distribution in both A- and C-tubules (Fig. 5C).
232 The frequency of the protofilament loss in the A-tubule seemingly varied
233 between the proximal and the distal regions of the centriole. To objectively show this
234 difference, we counted the number of missing protofilaments in four groups of axonemal
235 images that most likely represented distinct positions of the centriole: 1) (transition
236 zone) images with the characteristic star-like structure in the lumen; 2) (distal region)
237 images with distal appendages; 3) (proximal region) images with cartwheels; and 4)
238 (central region), images other than the above three groups (Table 2) (Geimer and
239 Melkonian, 2004; Le Guennec et al., 2021). The results showed that the protofilament
240 loss of the A-tubule was more frequently observed in the proximal region than in the

241 central or distal regions. No protofilament loss was observed in the transition zone. We
242 were unable to examine the regional difference of protofilament loss in the C-tubule,
243 because its image was obscured by electron-dense material near the proximal region
244 and was often missing in the distal region.
245
246 **Discussion**
247 In this study we demonstrated that two novel mutations in the γ-tubulin gene in
248 *Chlamydomonas* cause partial loss of protofilaments in centriolar triplet microtubules
249 while having relatively mild effects on the overall centriole structure. The
250 ultrastructural defects observed in the mutant centrioles highlight the crucial role of γ-
251 tubulin in maintaining the stability of triplet microtubules. This study provides the first
252 isolation and characterization of γ-tubulin mutants in *Chlamydomonas*.
253
254 **Effects of *bld13* mutations on the γ-TuRC assembly**
255 As γ-tubulin is an essential component of the microtubule-organizing center (MTOC),
256 required for fundamental cellular processes like cell division (Paz and Lüders, 2018;
257 Sulimenko et al., 2022), loss of γ-tubulin function results in lethality in many model
258 organisms (Sunkel et al., 1995; Hendrickson et al., 2001; Yuba-kubo et al., 2005;
259 Pastuglia et al. 2006). It is fortunate that the *bld13* mutants reported in this study have
260 only mild phenotypic aberrations and thus can provide a tractable system to dissect the
261 *in vivo* functions of γ-tubulin.
262 In many eukaryotes, γ-tubulin constitutes two kinds of complexes, one termed
263 the γ-tubulin small complex (γ-TuSCs) and the other termed the γ-tubulin ring complex
264 (γ-TuRC). The γ-TuSC is formed by association between γ-tubulin and two subunits,
265 GCP2 and GCP3; the γ-TuRCs is formed by oligomerization of γ-TuSCs and association
266 with GCP4~6 and MZT1 (Tovey and Conduit, 2018; Böhler et al., 2021). Because

267 *Chlamydomonas* has genes coding for homologs of GCP2~4 and MZT1, γ-tubulin of this
268 organism most likely also functions in microtubule nucleation by forming γ-TuRCs.
269 Both *bld13* mutations in the γ-tubulin gene cause single amino-acid
270 substitutions that do not change side-chain charge (Fig. 1D). Consistently, AlphaFold2
271 predicts no significant changes in the overall molecular structure (Fig. S1A). The
272 predicted minor structural effects of these mutations may be correlated with the mild
273 phenotypic abnormalities in the mutants: the mutant γ-tubulins localize to both
274 centrioles and the surrounding pericentriolar region as in wild-type cells (Silflow et al.,
275 1999), and cytoplasmic microtubules and ciliary axonemes are formed in most of the
276 mutant cells (Fig. 1-3). On closer inspection, however, the *bld13* mutations were
277 associated with three detectable abnormalities in microtubule structures in a subset of
278 cells. One abnormality was an increased population of cells exhibiting elevated numbers
279 of cytoplasmic microtubules, most clearly detected by staining for acetylated α-tubulin
280 (Fig. 4). A second abnormality, observed in a small fraction of cells, was the appearance
281 of cytoplasmic microtubules that lacked an obvious microtubule-organizing center (Fig.
282 4). A third abnormality was a partial loss of protofilaments in centriolar microtubules
283 (Fig. 5).
284 We speculate that these defects could result from some instability in the
285 association of the γ-tubulin molecules within the γ-TuRC. This is because the mutated
286 amino acid residues in both *bld13* mutants are located on the molecular surface at the
287 region where adjacent γ-tubulin molecules are presumed to interact within the complex
288 (Fig. S1B and C; Inclán and Nogales, 2000; Aldaz et al., 2005; Wieczorek et al., 2020). In
289 addition, AlphaMissense predicts that the equivalent substitutions in human γ-tubulin
290 are "likely pathogenic" (Cheng et al., 2023), further supporting the functional
291 importance of these residues. We propose that γ-tubulin molecules are stably held in the

292 complex by inter-subunit interaction at the contact sites, and the *bld13* mutations
293 partially disrupt this interaction.
294 Diploid analyses further support the dominant-negative mode of the *bld13*
295 mutations, consistent with the results of the γ-tubulin expression experiments (Fig. 2).
296 The presence of both wild-type and mutant γ-tubulin in heterozygous diploids suggest
297 that mutant subunits are incorporated into the γ-TuRC together with wild-type subunits,
298 thereby reducing the overall functional integrity of the complex. Moreover, the slightly
299 severer phenotype observed in the *bld13-1*/*bld13-2* homozygous diploid suggests that
300 the coexistence of the two mutations impairs inter-subunit contact surfaces more
301 strongly within the γ-TuRC. We speculate that weakened contact between γ-tubulins
302 may compromise γ-TuRC stability, leading to the defective cellular microtubule
303 organization and the partial loss of protofilaments observed in *bld13* mutants.
304 It remains unclear how the structural defects in the *bld13* γ-TuRC results in the
305 abnormal organization of the rootlet and non-rootlet microtubules (Fig. 4). Since other
306 centriole-deficient mutants we studied previously, *bld10* and *bld12*, also exhibited
307 abnormal rootlet microtubule arrangement (Matsuura et al., 2004; Nakazawa et al.,
308 2007), it is possible that the microtubule organization in *Chlamydomonas* is extremely
309 susceptible to the structural abnormality of the centriole.
310
311 **γ-tubulin functions in stabilization of centriolar microtubules**
312 The triplet microtubules of *bld13* centrioles frequently lack part of the protofilaments
313 (Fig. 5). This type of microtubule defects is unexpected because the lateral interaction
314 between protofilaments is likely essential for the stability of microtubules, and loss of a
315 protofilament would lead to depolymerization of whole microtubules (Gudimchuk and
316 McIntosh, 2021). However, the triplet microtubules in *bld13*, even when lacking
317 protofilaments, do not fully depolymerize. We speculate that these microtubules are

318 stabilized by some microtubule-associated structures or proteins, such as the A–C
319 linkers, microtubule inner proteins (MIPs), and the inner-scaffolds of the centriole (Li et
320 al., 2019; Le Guennec et al., 2020). It is interesting to note that the protofilament loss is
321 frequently observed in the region centered on A4 and the region C1-C7, where
322 protofilaments are apparently not associated with those structures or MIPs (Fig. 5C).
323 Protofilament loss in the A-tubule was observed more frequently in the
324 proximal region than in the central or distal region in both *bld13-1* and *bld13-2*
325 centrioles (Table 2), suggesting that the loss was caused by depolymerization from the
326 proximal end of previously formed protofilaments. *In vitro* studies have shown that the
327 γ-TuRC caps the microtubule minus end for a short period and suppresses both
328 polymerization and depolymerization (Wiese and Zheng, 2000; Berman et al., 2023). In
329 centriolar triplet microtubules *in vivo*, their minus ends may be mostly capped by the γ-
330 TuRC, since γ-tubulin has been localized near the proximal ends of the mature centrioles
331 in *Tetrahymena*, *Paramecium*, and mammals (Fuller et al., 1995; Klotz et al., 2003;
332 Joachimiak et al., 2018). Moreover, cryo-electron tomography of human procentrioles
333 has shown that the A-tubule proximal ends have a conical shape resembling the γ-TuRC-
334 capped microtubule end observed *in vitro* (Guichard et al., 2010). Thus, our observations
335 support the possibility that the γ-TuRC caps the proximal end of the A-tubule to
336 suppress depolymerization, and that this capping function may be compromised in the
337 *bld13* centrioles due to weakened interaction between γ-tubulin molecules.
338 Electron microscopy of the *bld13* centrioles revealed partial loss of
339 protofilaments also in the C-tubules (Fig. 5 B,C). The mechanism underlying formation
340 and maintenance of B- and C-tubules in centrioles remain poorly understood, although
341 several proteins, including δ-tubulin, ε-tubulin, and CPAP/SAS-4, have been implicated
342 in these processes (Hung et al., 2000; Dutcher, 2003; Gogendeau et al., 2011; Zheng et
343 al., 2016; Stathatos et al., 2021; Vásquez-Limeta et al., 2022; Guichard et al., 2023).

344 Unlike the A-tubule, which appears to have a capped proximal end, the B- and C-tubules
345 have open proximal ends, suggesting that their formation and stabilization rely on
346 mechanisms distinct from those of the A-tubule. Interestingly, however, a previous
347 study reported that overexpression of a γ-tubulin variant in *Tetrahymena* resulted in the
348 loss of B- and C-tubules in basal bodies (Joachimiak et al., 2018), raising the possibility
349 that γ-tubulin also contributes to the assembly or stability of these tubules. Consistent
350 with this idea, we observed protofilament loss from the centriolar C-tubule in the γ-
351 tubulin mutants. One possibility is that γ-TuRCs localized to the outer wall of the
352 centriole contribute to the stabilization of the C-tubule, and possibly the B-tubule as well
353 (Schweizer and Lüders, 2021; Kalbfuss and Gönczy, 2023).
354 In summary, we found that the *bld13* mutations in γ-tubulin lead to a partial loss
355 of protofilaments of centriolar triplet microtubules, while the triplet structure remains
356 stable even when some protofilaments are lost. The loss of protofilaments appears to
357 proceed from the proximal end, potentially due to reduced minus-end capping by the γ-
358 TuRC containing *bld13* γ-tubulin. Our findings have thus highlighted a potential role for
359 γ-tubulin and the γ-TuRC in the stabilization of the minus end of the centriole
360 microtubules, in addition to their established function in initiating tubulin
361 polymerization.
362
363
364 **Materials and methods**
365 ***Chlamydomonas reinhardtii* strains**
366 The wild type strains CC124 and CC125, and S1-D2 were obtained from the
367 *Chlamydomonas* Resource Center (University of Minnesota). The mutant *bld13-*
368 *1* and *bld13-2* were isolated in this study by screening CC125 cells treated with N-
369 methyl-N'-nitro-N-nitrosoguanidine (MNNG) or irradiated with UV, respectively. The

370 isolated strains were then backcrossed twice with wild-type, and the resulting F2
371 progeny were used for all subsequent analyses. The diploid strains (WT/WT, WT/*bld13-*
372 *1*, WT/*bld13-2*, *bld13-1*/*bld13-2*) were produced by crossing two strains with different
373 antibiotic resistance: hygromycin and paromomycin resistance, each conferred by
374 transformation with a plasmid pHyg3 carrying aphVII or pSI103 carrying aphVIII gene
375 by electroporation (Ebersold, 1967; Berthold et al., 2002; Sizova et al., 2001; Yamano et
376 al., 2013). Cells were grown in Tris-acetate-phosphate (TAP) medium with constant
377 illumination (Gorman and Levine, 1965).
378
379 **Expression of HA-tagged γ-tubulin in *Chlamydomonas***
380 Genome fragments containing the γ-tubulin gene
381 (Cre06.g299300v5, https://phytozome-next.jgi.doe.gov/) were amplified by PCR with
382 the primers γ-tub-F (5'-AACTCCCTCACCACCCAGTCA-3') and γ-tub-R (5'-
383 TTTCATTAGGGACCAGGTTAG-3') using genomic DNA of the wild-type, *bld13-1* or *bld13-*
384 *2*. The forward primer (γ-tub-F) was designed to amplify approximately 500 bp
385 upstream of the 5'UTR region of the γ-tubulin gene, thereby including its putative native
386 promoter region within the amplified fragment. The amplified fragments were cloned
387 into pCR-Blunt II-TOPO vector (Invitrogen). Into this plasmid, a SpeI fragment
388 containing the aphVII gene excised from pHyg3 was inserted at the SpeI site, and a
389 fragment containing 3×HA-tag sequences digested with NruI/ScaI from p3×HA (Silflow
390 et al., 2001) was inserted at the site adjacent to the stop codon of the γ-tubulin gene.
391 These plasmids were introduced into the wild-type, *bld13-1* or *bld13-2* cells by
392 electroporation using the NEPA21 electroporator (Nepa Gene, Japan) (Yamano et al.,
393 2013). Of the transformants that display resistance to hygromycin, the clones that
394 express the HA-tagged γ-tubulin were screened by Western blotting using anti-HA
395 antibody (3F10, Roche).

396

397 **Genetic mapping and whole genome sequencing**

398 The mutations *bld13-1* and *bld13-2* were mapped to a region containing the γ-tubulin
399 gene on Chromosome 6 by amplified-fragment-length polymorphism (AFLP)-based
400 analyses of progenies from the mating of these mutants with S1-D2 (Kathir et al., 2003;
401 Nakazawa et al., 2007). Recombination frequencies between each mutation and genetic
402 markers on Chromosome 6 were determined by detecting polymorphisms in PCR
403 products. The genetic markers used were as follows: 19-559 (5'-
404 CAGTGTGTAGGGTTGAGCACAGGA-3', 5'-CAGCCGGAGATGTTTACGTTTGAG-3')
405 190065 (5'-GGGGCACTGACGTCAGGCAAG-3', 5'-GCAAAGCGTCTAGCCTGGACGAA-3', 5'-
406 GGATACTGGACTACTTTCACGCTGCA-3'), 190071 (5'-GGCCCAGTCGATGCTGGTGTTCGG-
407 3', 5'-GTCTGGGTCGGCGCCCTTGAGA-3', 5'-GGGGCACACATGATGAGAGGTGCG-3'), TUG
408 (5'-GTCGCCAGGAATTTTGCCCCTGG-3', 5'-GCGCGCCTGGCGGTAGCACATA-3', 5'-
409 AGCAGCGCTATGTTCGCTTCCCC-3'), 19-1050 (5'-AGGCAGGGGAGACATAGGTAGGAG-3',
410 5'-GACCCTATGACCACCATCTGTTCC-3'), 9-0003 (5'-GTAGCACCATATGGGTGGAGTGG-3',
411 5'-AGAACTGCGCCAAGATTTGCACG-3'). Of these markers, no recombinants were
412 detected between the mutations and markers 190071, TUG, and 19-1050 in 188 mutant
413 progenies examined.

414 For whole genome sequencing, genomic DNA was prepared using the DNeasy
415 Plant Mini kit (QIAGEN) from *bld13-1* cells pretreated with gametolysin to remove the
416 cell wall (Kindle, 1990). A total of 100 ng of genomic DNA was fragmented to an average
417 size of ~350 bp using a Covaris sonicator. Sequence libraries were constructed from the
418 DNA fragments using the TruSeq Nano DNA library prep kit (Illumina), essentially
419 following the manufacturer's instructions. To minimize PCR amplification bias, the
420 number of PCR cycles in the amplification enrichment step was reduced to four. The
421 generated library was evaluated with the Bioanalyzer (Agilent) and then sequenced on a

422 HiSeq 2500 (Illumina) in a 101 x 101 paired-end format.

423 The sequence reads were aligned onto the *Chlamydomonas* genome sequence
424 version 5.3.1 (Creinhardtii_236.fa.gz) downloaded from the Joint Genome Institute (JGI)
425 (https://phytozome.jgi.doe.gov/pz/portal) using bowtie2 (bowtie-
426 biosourceforge.net/bowtie2/index.shtml). The *bld13-1* mutation was identified by
427 comparing the genome sequence of *bld13-1* with that of CC124 and CC503 focusing on
428 the mapped ~400-kb region on Chromosome 6. The *bld13-2* mutation was identified by
429 PCR amplification and sequencing of the γ-tubulin gene in the *bld13-2* genome.

430

431 **Western blot analysis**

432 For immunoblotting, whole-cell extracts (10 μg/lane) from *Chlamydomonas* cells were
433 separated by SDS-PAGE and transferred to Immobilon-P membranes (Millipore) as
434 described in Noga et al., 2022. Anti-HA antibody bound to the membrane were detected
435 with goat anti-rat IgG conjugated with horseradish peroxidase (HRP) (Sigma).

436

437 **Immunofluorescence microscopy**

438 *Chlamydomonas* cells were fixed and prepared for antibody staining as described
439 previously (Arakaki et al., 2017). Anti-HA antibody (3F10, Roche), anti-α-tubulin
440 antibody (B-5-1-2, Sigma), Rabbit anti-SAS-6 antibody (Nakazawa et al., 2007), and anti-
441 acetylated α-tubulin antibody (6-11B-1, Sigma) were used as primary antibodies. Goat
442 anti-mouse IgG conjugated with Alexa Fluor 647 (Thermo Fisher Scientific), goat anti-
443 mouse IgG(H+L) cross-adsorbed secondary antibody conjugated with Alexa Fluor 488
444 (Thermo Fisher Scientific), goat anti-rat IgG conjugated with Alexa Fluor 488 (Thermo
445 Fisher Scientific), and goat anti-rabbit IgG conjugated with Alexa Fluor 546 (Thermo
446 Fisher Scientific) were used as secondary antibodies. Images were acquired using a
447 Nikon AX confocal microscope equipped with an NSPARC super-resolution detector

448 (Nikon Instruments Inc.). For the observation of cytoplasmic microtubules, Z-stacks
449 were collected at 0.15-μm intervals, and Z-projected images were generated using
450 maximum-intensity projection of 40-50 optical sections.
451
452 **Quantification of microtubule defects**
453 For quantification of microtubule organization (Fig. 4), Z-projected immunofluorescence
454 images of cells stained with anti–acetylated α-tubulin antibody (Fig. 4A) or anti–α-
455 tubulin antibody (Fig. 4B) were analyzed. Cells were categorized into four groups based
456 on the number and organization of stained microtubules: cells with three or fewer
457 microtubules (≤3 MTs), cells with four microtubules (4 MTs), cells with five or more
458 microtubules (≥5 MTs), and cells with cage-like microtubules that did not originate from
459 an obvious organizing center (CL). Statistical analysis was performed using Fisher's
460 exact test in GraphPad Prism to compare the distribution of microtubule categories
461 between wild-type and mutant strains. For each strain, more than 120 cells were
462 randomly selected and manually scored. The statistical power of 0.8 or higher was
463 confirmed for each comparison in a post hoc manner using G*Power (Faul et al., 2007).
464
465 **Electron microscopy**
466 Logarithmically growing cells were prefixed with 2% glutaraldehyde in 0.1 M S-collidine
467 buffer for 1–2 hr at 0ºC and postfixed with 1% OsO4 in the same buffer for 1-2 hr
468 (Wright et al., 1983). The specimens were then dehydrated and embedded in EPON 812.
469 Thin sections (50–70 nm) were stained with aqueous uranyl acetate and Reynold's lead
470 citrate and observed with JEM-1400plus at 80 kV or JEM-1230R at 100 kV (JEOL).
471
472 **Analysis of protofilament loss in centriolar triplet microtubules**

473 To evaluate triplet microtubule integrity, we collected electron microscope images
474 of triplet microtubules in the distal, central and proximal regions of the A tubule, and the
475 central region of the C-tubule of *bld13-1* and *bld13-2* centrioles (Table 2) based on the
476 clarity of the protofilaments. Potential intrinsic variation among the nine triplets within
477 each centriole was not considered during image selection. To evaluate protofilament
478 loss, each tubule image was divided into sectors (12 for the A-tubule and 6 for the C-
479 tubule), and the number of missing protofilaments in each sector was scored (Fig. 5C).
480 Missing protofilaments were scored in sectors rather than in numbered protofilaments
481 because the images often lacked sufficient resolution to identify specific protofilament
482 numbers. The B-tubule did not show any protofilament loss.
483 To assess whether the distribution of protofilament loss across sectors was
484 uniform or showed a preferential orientation, circular statistics were employed.
485 Specifically, the Hodges-Ajne test was performed for each genotype to test for
486 uniformity on the circular data using a custom MATLAB script. Sample sizes were
487 initially determined based on experimental feasibility. The statistical power of 0.8 or
488 higher was confirmed for each comparison in a post-hoc manner using G*Power (Faul et
489 al., 2007).
490
491
492 **Acknowledgements**
493 We thank Dr. Ritsu Kamiya (Chuo University) for critically reading the manuscript, Dr.
494 Takako Kato-Minoura (Chuo Univ.) and OIST Imaging Section for use of electron
495 microscopes, OIST Memory Research Unit, OIST Evolution, Cell biology, Symbiosis Unit,
496 OIST Membrenology Unit, Dr. Midori Ohta (OIST), Dr. Petra Svetlikova (OIST), Dr.
497 Yohsuke Moriyama (OIST) and Dr. Akane Furuta (NICT) for helpful advice and fruitful
498 discussions. This work was supported by JSPS KAKENHI (16J40154 to YN, 23K23905 to

KW, and 21K06257 and 24K02055 to MH). This work was also supported in part by NIBB Collaborative Research Program (14733) to KW.

Author contributions

Conceptualization: Yuki Nakazawa, Mao Horii, Masafumi Hirono

Methodology: Yuki Nakazawa, Mao Horii, Masafumi Hirono

Investigation: Yuki Nakazawa, Naoto Kubota, Mao Horii, Akira Noga, Yoshikazu Koike, Katsushi Yamaguchi, Shuji Shigenobu

Validation: Yuki Nakazawa

Formal analysis: Yuki Nakazawa, Hideo Dohra

Resources: Yuki Nakazawa, Hideo Dohra, Katsushi Yamaguchi, Shuji Shigenobu, Ken-ichi Wakabayashi, Masafumi Hirono

Data curation: Yuki Nakazawa, Hiroko Kawai-Toyooka, Masafumi Hirono

Writing – original draft: Yuki Nakazawa, Masafumi Hirono

Writing – review & editing: Yuki Nakazawa, Masafumi Hirono, Ken-ichi Wakabayashi

Visualization: Yuki Nakazawa, Hiroko Kawai-Toyooka

Supervision: Masafumi Hirono

Project administration: Yuki Nakazawa, Masafumi Hirono

Funding acquisition: Yuki Nakazawa, Ken-ichi Wakabayashi, Masafumi Hirono

Competing interests

The authors declare no competing or financial interests.

Data availability

The datasets supporting the findings of this study will be deposited in Dryad upon acceptance and will be made publicly available prior to publication.

528 **References**

529 Aldaz H., Rice L.M., Stearns T., and Agard D.A. (2005). Insights into microtubule
530 nucleation from the crystal structure of human gamma-tubulin. *Nature* **435**, 523-527.
531 doi: 10.1038/nature03586.
532
533 Arakaki, Y., Fujiwara, T., Kawai-Toyooka, H., Kawafune, K., Featherston, J., Durand, P. M.,
534 Miyagishima, S. Y., and Nozaki, H. (2017). Evolution of cytokinesis-related protein
535 localization during the emergence of multicellularity in volvocine green algae. BMC Evol.
536 Biol. 17, 243. doi: 10.1186/s12862-017-1091-z
537
538 Azimzadeh J., and Marshall W.F. (2010). Building the centriole. *Curr. Biol.* **20**, R816-25.
539 doi: 10.1016/j.cub.2010.08.010.
540
541 Bahtz R., Seidler J., Arnold M., Haselmann-Weiss U., Antony C., Lehmann W.D., and
542 Hoffmann I. (2012). GCP6 is a substrate of Plk4 and required for centriole duplication. *J.*
543 *Cell Sci.* **125**, 486-496. doi: 10.1242/jcs.093930.
544
545 Berman A.Y., Wieczorek M., Aher A., Olinares P.D.B., Chait B.T., and Kapoor T.M. (2023).
546 A nucleotide binding-independent role for γ-tubulin in microtubule capping and cell
547 division. *J. Cell Biol.* **222**, e202204102. doi: 10.1083/jcb.202204102.
548
549 Berthold P., Schmitt R., and Mages W. (2002). An engineered Streptomyces
550 hygroscopicus aph 7" gene mediates dominant resistance against hygromycin B in
551 *Chlamydomonas reinhardtii*. *Protist* **153**, 401-412. doi: 10.1078/14344610260450136.
552
553 Böhler A., Vermeulen B.J.A., Würtz M., Zupa E., Pfeffer S., and Schiebel E. (2021). The

554 gamma-tubulin ring complex: Deciphering the molecular organization and assembly
555 mechanism of a major vertebrate microtubule nucleator. *Bioessays* **43**, e2100114. doi:
556 10.1002/bies.202100114.
557
558 Cota R.R., Teixidó-Travesa N., Ezquerra A., Eibes S., Lacasa C., Roig J., and Lüders J.
559 (2017). MZT1 regulates microtubule nucleation by linking γTuRC assembly to adapter-
560 mediated targeting and activation. *J. Cell Sci.* **130**, 406-419. doi: 10.1242/jcs.195321.
561
562 Cheng J., Novati G., Pan J., Bycroft C., Žemgulytė A., Applebaum T., Pritzel A., Wong L.H.,
563 Zielinski M., Sargeant T., Schneider R.G., Senior A.W., Jumper J., Hassabis D., Kohli P., and
564 Avsec Ž. (2023). Accurate proteome-wide missense variant effect prediction with
565 AlphaMissense. *Science* **381**, eadg7492. doi: 10.1126/science.adg7492.
566
567 Dammermann A., Müller-Reichert T., Pelletier L., Habermann B., Desai A., and Oegema K.
568 (2004). Centriole assembly requires both centriolar and pericentriolar material
569 proteins. *Dev. Cell* **7**, 815-829. doi: 10.1016/j.devcel.2004.10.015.
570
571 Dutcher S.K., and Trabuco E.C. (1998). The UNI3 gene is required for assembly of basal
572 bodies of *Chlamydomonas* and encodes delta-tubulin, a new member of the tubulin
573 superfamily. *Mol. Biol. Cell* **9**, 1293-1308. doi: 10.1091/mbc.9.6.1293.
574
575 Dutcher S.K. (2003). Long-lost relatives reappear: identification of new members of the
576 tubulin superfamily. *Curr. Opin. Microbiol.* **6**, 634-640. doi: 10.1016/j.mib.2003.10.016.
577
578 Ebersold W.T. (1967). *Chlamydomonas reinhardi*: heterozygous diploid strains. *Science*
579 **157**, 447-449. doi: 10.1126/science.157.3787.447.

580

581 Ehler L.L., Holmes J.A., and Dutcher S.K. (1995). Loss of spatial control of the mitotic
582 spindle apparatus in a *Chlamydomonas reinhardtii* mutant strain lacking basal bodies.
583 *Genetics* **141**, 945-960. doi: 10.1093/genetics/141.3.945.

584

585 Faul F, Erdfelder E, Lang AG, Buchner A. (2007). G*Power 3: a flexible statistical power
586 analysis program for the social, behavioral, and biomedical sciences. *Behav. Res. Methods*
587 **39**, 175-91. doi: 10.3758/bf03193146.

588

589 Fuller S.D., Gowen B.E., Reinsch S., Sawyer A., Buendia B., Wepf R., and Karsenti E.
590 (1995). The core of the mammalian centriole contains gamma-tubulin. *Curr. Biol.* **5**,
591 1384-1393. doi: 10.1016/s0960-9822(95)00276-4.

592

593 Geimer S., and Melkonian M. (2004). The ultrastructure of the *Chlamydomonas*
594 *reinhardtii* basal apparatus: identification of an early marker of radial asymmetry
595 inherent in the basal body. *J. Cell Sci.* **117**, 2663-2674. doi: 10.1242/jcs.01120.

596

597 Gogendeau D., Hurbain I., Raposo G., Cohen J., Koll F., and Basto R. (2011). Sas-4 proteins
598 are required during basal body duplication in Paramecium. *Mol. Biol. Cell.* **22**, 1035-
599 1044. doi: 10.1091/mbc.E10-11-0901.

600

601 Gorman D.S., and Levine R.P. (1965). Cytochrome f and plastocyanin: their sequence in
602 the photosynthetic electron transport chain of *Chlamydomonas reinhardii*. *Proc. Natl.*
603 *Acad. Sci. USA* **54**, 1665-1669. doi: 10.1073/pnas.54.6.1665.

604

605 Gudimchuk N.B., and McIntosh J.R. (2021). Regulation of microtubule dynamics,

606 mechanics and function through the growing tip. *Nat. Rev. Mol. Cell Biol.* **22**, 777-795.
607 doi: 10.1038/s41580-021-00399-x.
608
609 Guichard P., Chrétien D., Marco S., and Tassin A.M. (2010). Procentriole assembly
610 revealed by cryo-electron tomography. *EMBO J.* **29**, 1565-1572. doi:
611 10.1038/emboj.2010.45.
612
613 Guichard P., Laporte M.H., and Hamel V. (2023). The centriolar tubulin code. *Semin. Cell*
614 *Dev. Biol.* **137**, 16-25. doi: 10.1016/j.semcdb.2021.12.001.
615
616 Hendrickson T.W., Yao J., Bhadury S., Corbett A.H., and Joshi H.C. (2001). Conditional
617 mutations in gamma-tubulin reveal its involvement in chromosome segregation and
618 cytokinesis. *Mol. Biol. Cell*. **12**, 2469-81. doi: 10.1091/mbc.12.8.2469.
619
620 Hiraki M., Nakazawa Y., Kamiya R., and Hirono M. (2007). Bld10p constitutes the
621 cartwheel-spoke tip and stabilizes the 9-fold symmetry of the centriole. *Curr. Biol.* **17**,
622 1778-1783. doi: 10.1016/j.cub.2007.09.021.
623
624 Holmes J.A., and Dutcher S.K. (1989). Cellular asymmetry in *Chlamydomonas reinhardtii.*
625 *J. Cell Sci.* **94**, 273-285. doi: 10.1242/jcs.94.2.273.
626
627 Hung L.Y., Tang C.J. and Tang T.K. (2000). Protein 4.1 R-135 interacts with a novel
628 centrosomal protein (CPAP) which is associated with the gamma-tubulin complex. *Mol.*
629 *Cell Biol.* **20**, 7813-7825. doi: 10.1128/MCB.20.20.7813-7825.2000.
630
631 Inclán Y.F., and Nogales E. (2001). Structural models for the self-assembly and

632 microtubule interactions of gamma-, delta- and epsilon-tubulin. *J. Cell Sci.* **114**, 413-422.
633 doi: 10.1242/jcs.114.2.413.
634
635 Joachimiak E., Jerka-Dziadosz M., Krzemień-Ojak Ł., Wacławek E., Jedynak K., Urbanska
636 P., Brutkowski W., Sas-Nowosielska H., Fabczak H., Gaertig J., and Wloga D. (2018).
637 Multiple phosphorylation sites on γ-tubulin are essential and contribute to the
638 biogenesis of basal bodies in Tetrahymena. *J. Cell. Physiol.* **233**, 8648–8665. doi:
639 10.1002/jcp.26742.
640
641 Jumper J., Evans R., Pritzel A., Green T., Figurnov M., Ronneberger O., Tunyasuvunakool
642 K., Bates R., Žídek A., Potapenko A., Bridgland A., Meyer C., Kohl S.A.A., Ballard A.J., Cowie
643 A., Romera-Paredes B., Nikolov S., Jain R., Adler J., Back T., Petersen S., Reiman D., Clancy
644 E., Zielinski M., Steinegger M., Pacholska M., Berghammer T., Bodenstein S., Silver D.,
645 Vinyals O., Senior A.W., Kavukcuoglu K., Kohli P., and Hassabis D. (2021). Highly accurate
646 protein structure prediction with AlphaFold. *Nature* ***596***, 583-589. doi:
647 10.1038/s41586-021-03819-2.
648
649 Kalbfuss N., and Gönczy P. (2023). Towards understanding centriole elimination. *Open*
650 *Biol.* 13, 230222. doi: 10.1098/rsob.230222.
651
652 Kathir P., LaVoie M., Brazelton W.J., Haas N.A., and Lefebvre P.A., Silflow CD (2003).
653 Molecular map of the *Chlamydomonas reinhardtii* nuclear genome. *Eukaryot. Cell* 2, 362-
654 379. doi: 10.1128/EC.2.2.362-379.2003.
655
656 Kindle K.L. (1990). High-frequency nuclear transformation of *Chlamydomonas*
657 *reinhardtii. Proc. Natl. Acad. Sci. USA* **87**, 1228-1232. doi: 10.1073/pnas.87.3.1228.

658

659 Klotz C., Ruiz F., Garreau de Loubresse N., Wright M., Dupuis-Williams P. and Beisson J.
660 (2003). Gamma-tubulin and MTOCs in Paramecium. *Protist* **154**, 193-209. doi:
661 10.1078/143446103322166509.
662

663 Laporte M.H., Gambarotto D., Bertiaux É., Bournonville L., Louvel V., Nunes J.M., Borgers
664 S., Hamel V., and Guichard P. (2024). Time-series reconstruction of the molecular
665 architecture of human centriole assembly. *Cell* **187**, 2158-2174.e19. doi:
666 10.1016/j.cell.2024.03.025.
667

668 Le Guennec M., Klena N., Gambarotto D., Laporte M.H., Tassin A.M., van den Hoek H.,
669 Erdmann P.S., Schaffer M., Kovacik L., Borgers S., Goldie K.N., Stahlberg H., Bornens M.,
670 Azimzadeh J., Engel B.D., Hamel V., and Guichard P. (2020). A helical inner scaffold
671 provides a structural basis for centriole cohesion. *Sci. Adv.* **6**, eaaz4137.
672

673 Le Guennec M., Klena N., Aeschlimann G., Hamel V., and Guichard P. (2021). Overview of
674 the centriole architecture. *Curr. Opin. Struct. Biol.* **66**, 58-65. doi:
675 10.1126/sciadv.aaz4137.
676

677 Li J.B., Gerdes J.M., Haycraft C.J., Fan Y., Teslovich T.M., May-Simera H., Li H., Blacque O.E.,
678 Li L., Leitch C.C., Lewis R.A., Green J.S., Parfrey P.S., Leroux M.R., Davidson W.S., Beales
679 P.L., Guay-Woodford L.M., Yoder B.K., Stormo G.D., Katsanis N., and Dutcher S.K. (2004).
680 Comparative genomics identifies a flagellar and basal body proteome that includes the
681 BBS5 human disease gene. *Cell* **117**, 541-52. doi: 10.1016/s0092-8674(04)00450-7.
682

683 Li S., Fernandez J.J., Marshall W.F., and Agard D.A. (2019). Electron cryo-tomography

684 provides insight into procentriole architecture and assembly mechanism. *Elife* **8**,
685 e43434. doi: 10.7554/eLife.43434.
686
687 Linck R.W., and Stephens R.E. (2007). Functional protofilament numbering of ciliary,
688 flagellar, and centriolar microtubules. *Cell Motil. Cytoskeleton* **64**, 489-495. doi:
689 10.1002/cm.20202.
690
691 Liu P., Würtz M., Zupa E., Pfeffer S., and Schiebel E. (2021). Microtubule nucleation: The
692 waltz between γ-tubulin ring complex and associated proteins. *Curr. Opin. Cell Biol.* **68**,
693 124-131. doi: 10.1016/j.ceb.2020.10.004.
694
695 Matsuura K., Lefebvre P.A., Kamiya R., and Hirono M. (2004). Bld10p, a novel protein
696 essential for basal body assembly in *Chlamydomonas*: localization to the cartwheel, the
697 first ninefold symmetrical structure appearing during assembly. *J. Cell Biol.* **165**, 663-
698 671. doi: 10.1083/jcb.200402022.
699
700 Mukhopadhyay S., Gao Q., Manna T.K., and Schiebel E. (2026). The γ-TuRC: mastermind
701 of multipurpose actions at the centrosome. Cell. Mol. Life Sci. 83, 120. doi:
702 10.1007/s00018-026-06080-w.
703
704 Nakazawa Y., Hiraki M., Kamiya R., and Hirono M. (2007). SAS-6 is a cartwheel protein
705 that establishes the 9-fold symmetry of the centriole. *Curr. Biol.* **17**, 2169-2174. doi:
706 10.1016/j.cub.2007.11.046.
707
708 Noga A., Horii M., Goto Y., Toyooka K., Ishikawa T., and Hirono M. (2022).
709 Bld10p/Cep135 determines the number of triplets in the centriole independently of the

710 cartwheel. *EMBO J.* **41**, e104582. doi: 10.15252/embj.2020104582.

711

712 Oakley B.R., Paolillo V., and Zheng Y. (2015). γ-Tubulin complexes in microtubule

713 nucleation and beyond. *Mol. Biol. Cell* **26**, 2957-2962. doi: 10.1091/mbc.E14-11-1514.

714

715 Osinka A., Poprzeczko M., Zielinska M.M., Fabczak H., Joachimiak E., and Wloga D. (2019).

716 Ciliary Proteins: Filling the Gaps. Recent Advances in Deciphering the Protein

717 Composition of Motile Ciliary Complexes. *Cells* **8**, 730. doi: 10.3390/cells8070730.

718

719 Pastuglia M., Azimzadeh J., Goussot M., Camilleri C., Belcram K., Evrard J.L., Schmit A.C.,

720 Guerche P., and Bouchez D. (2006). Gamma-tubulin is essential for microtubule

721 organization and development in Arabidopsis. *Plant Cell* **18**, 1412-25. doi:

722 10.1105/tpc.105.039644.

723

724 Paz J., and Lüders J. (2018). Microtubule-Organizing Centers: Towards a Minimal Parts

725 List. *Trends Cell Biol.* **28**, 176-187. doi: 10.1016/j.tcb.2017.10.005.

726

727 Pazour G.J., Agrin N., Leszyk J., and Witman G.B. (2005). Proteomic analysis of a

728 eukaryotic cilium. *J. Cell Biol.* **170**, 103-13. doi: 10.1083/jcb.200504008.

729

730 Ruiz F., Beisson J., Rossier J., and Dupuis-Williams P. (1999). Basal body duplication in

731 Paramecium requires gamma-tubulin. *Curr. Biol.* **9**, 43-46. doi: 10.1016/s0960-

732 9822(99)80045-1.

733

734 Schweizer N., Haren L., Dutto I., Viais R., Lacasa C., Merdes A., and Lüders J. (2021). Sub-

735 centrosomal mapping identifies augmin-γTuRC as part of a centriole-stabilizing scaffold.

736 *Nat. Commun.* **12**, 6042. doi: 10.1038/s41467-021-26252-5.

737

738 Schweizer N., and Lüders J. (2021). From tip to toe - dressing centrioles in γTuRC. *J. Cell*
739 *Sci.* **134**, jcs258397. doi: 10.1242/jcs.258397.

740

741 Shang Y., Li B., and Gorovsky M.A. (2002). Tetrahymena thermophila contains a
742 conventional gamma-tubulin that is differentially required for the maintenance of
743 different microtubule-organizing centers. *J. Cell Biol.* **158**, 1195-1206. doi:
744 10.1083/jcb.200205101.

745

746 Sievers F., and Higgins D.G. (2014). Clustal omega. *Curr. Protoc. Bioinformatics* **48**,
747 3.13.1-3.13.16. doi: 10.1002/0471250953.bi0313s48.

748

749 Silflow C.D., Liu B., LaVoie M., Richardson E.A., and Palevitz B.A. (1999). Gamma-tubulin
750 in *Chlamydomonas*: characterization of the gene and localization of the gene product in
751 cells. *Cell Motil. Cytoskeleton* **42**, 285-97. doi: 10.1002/(SICI)1097-
752 0169(1999)42:4<285::AID-CM3>3.0.CO;2-Z.

753

754 Silflow C.D., LaVoie M., Tam L.W., Tousey S., Sanders M., Wu W., Borodovsky M., and
755 Lefebvre P.A. (2001). The Vfl1 Protein in *Chlamydomonas* localizes in a rotationally
756 asymmetric pattern at the distal ends of the basal bodies. *J. Cell Biol.* **153**, 63-74. doi:
757 10.1083/jcb.153.1.63.

758

759 Sizova I., Fuhrmann M., and Hegemann P. (2001). A Streptomyces rimosus aphVIII gene
760 coding for a new type phosphotransferase provides stable antibiotic resistance to
761 *Chlamydomonas reinhardtii*. *Gene* **277**, 221-229. doi: 10.1016/s0378-1119(01)00616-3.

762

763 Stathatos G.G., Dunleavy J.E.M., Zenker J., and O'Bryan M.K. (2021). Delta and epsilon
764 tubulin in mammalian development. *Trends Cell Biol.* **31**, 774-787. doi:
765 10.1016/j.tcb.2021.03.010.

766

767 Sulimenko V., Dráberová E., and Dráber P. (2022). γ-Tubulin in microtubule nucleation
768 and beyond. *Front. Cell Dev. Biol.* **10**, 880761. doi: 10.3389/fcell.2022.880761.

769

770 Sunkel C.E., Gomes R., Sampaio P., Perdigão J., and González C. (1995). Gamma-tubulin is
771 required for the structure and function of the microtubule organizing centre in
772 Drosophila neuroblasts. *EMBO J.* **14**, 28-36. doi: 10.1002/j.1460-2075.1995.tb06972.x.

773

774 Thawani A., and Petry S. (2021). Molecular insight into how γ-TuRC makes
775 microtubules. *J. Cell Sci.* **134**, jcs245464. doi: 10.1242/jcs.245464.

776

777 Tovey C.A., and Conduit P.T. (2018). Microtubule nucleation by γ-tubulin complexes and
778 beyond. *Essays Biochem.* **62**, 765-780. doi: 10.1042/EBC20180028.

779

780 Vásquez-Limeta A., Lukasik K., Kong D., Sullenberger C., Luvsanjav D., Sahabandu N.,
781 Chari R., and Loncarek J. (2022). CPAP insufficiency leads to incomplete centrioles that
782 duplicate but fragment. *J. Cell Biol.* **221**, e202108018. doi: 10.1083/jcb.202108018.

783

784 Wang J.T., and Stearns T. (2017). The ABCs of Centriole Architecture: The Form and
785 Function of Triplet Microtubules. *Cold Spring Harb. Symp. Quant. Biol.* **82**, 145-155. doi:
786 10.1101/sqb.2017.82.034496.

787

788 Wieczorek M., Urnavicius L., Ti S.C., Molloy K.R., Chait B.T., and Kapoor T.M.(2020).
789 Asymmetric Molecular Architecture of the Human γ-Tubulin Ring Complex. *Cell* **180**,
790 165-175.e16. doi: 10.1016/j.cell.2019.12.007.
791
792 Wiese C., and Zheng Y. (2000). A new function for the gamma-tubulin ring complex as a
793 microtubule minus-end cap. *Nat. Cell Biol.* **2**, 358-364. doi: 10.1038/35014051.
794
795 Wright R.L., Salisbury J., and Jarvik J.W. (1985). A nucleus-basal body connector in
796 *Chlamydomonas reinhardtii* that may function in basal body localization or segregation. *J.*
797 *Cell Biol.* **101**, 1903-1912. doi: 10.1083/jcb.101.5.1903.
798
799 Wu J., and Akhmanova A. (2017). Microtubule-Organizing Centers. *Annu. Rev. Cell Dev.*
800 *Biol.* **33**, 51-75. doi: 10.1146/annurev-cellbio-100616-060615.
801
802 Yamano T., Iguchi H., and Fukuzawa H. (2013). Rapid transformation of *Chlamydomonas*
803 *reinhardtii* without cell-wall removal. *J. Biosci. Bioeng.* **115**, 691-694. doi:
804 10.1016/j.jbiosc.2012.12.020.
805
806 Yuba-Kubo A., Kubo A., Hata M., and Tsukita S. (2005). Gene knockout analysis of two
807 gamma-tubulin isoforms in mice. *Dev. Biol.* **282**, 361-73. doi:
808 10.1016/j.ydbio.2005.03.031.
809
810 Zheng X., Ramani A., Soni K., Gottardo M., Zheng S., Ming Gooi L., Li W., Feng S.,
811 Mariappan A., Wason A., Widlund P., Pozniakovsky A., Poser I., Deng H., Ou G., Riparbelli
812 M., Giuliano C., Hyman A.A., Sattler M., Gopalakrishnan J., and Li H. (2016). Molecular
813 basis for CPAP-tubulin interaction in controlling centriolar and ciliary length. *Nat.*

Commun. **7**, 11874.

Zupa E., Liu P., Würtz M., Schiebel E., and Pfeffer S. (2021). The structure of the γ-TuRC: a 25-years-old molecular puzzle. *Curr. Opin. Struct. Biol.* **66**, 15-21. doi: 10.1038/ncomms11874.

820 Table 1. Abnormal nuclear segregation in the *bld13* mutants.

Strain	Number of nuclei/cell (n>2200)			
	0	1	2 or 3	
wild type	0.61	99.30	0.09	
bld12-1	3.70	90.20	6.11	
bld13-1	1.24	95.34	3.43	
bld13-2	0.64	98.39	0.97	(%)

821

822

823 Table 2. Frequencies of triplet images with partial protofilament loss (%).

824 Percentages indicate the proportion of observed triplet microtubule images showing

825 loss of one or more protofilaments.

Strain		Regions in longitudinal axis of the centriole				
		Transition zone n>60	Distal n>50	Central n>50	Proximal n>30	
Wild type	A-tubule	ND	0.0	0.0	0.0	
	C-tubule	ND	ND	0.0	ND	
bld13-1	A-tubule	0.0	4.0	23.3	37.1	
	C-tubule	ND	ND	12.3	ND	
bld13-2	A-tubule	0.0	0.0	9.6	16.7	
	C-tubule	ND	ND	23.9	ND	(%)

826

827 **Figure legends**

828 **Fig. 1.**

829 Novel *Chlamydomonas* mutants *bld13-1* and *bld13-2*. (A) Phase contrast images of wild-
830 type, *bld13-1* and *bld13-2* cells. Both *bld13* mutants contain cells with no or one cilium in
831 addition to cells with two cilia. Scale bar: 5 μm. (B) Percentages of cells with zero, one, or
832 two cilia in wild type (WT), *bld13-1*, and *bld13-2*. Statistical analysis was performed
833 using Fisher's exact test (***P<0.001; n>1500). (C) A genetic map showing a part of
834 Linkage Group VI. The *bld13-1* and *bld13-2* mutations were mapped to an ~400-kb
835 region in this linkage group by AFLP-based analyses. The upper line shows the
836 corresponding locus on the genetic map constructed by Kathir et al. (Kathir et al., 2003).
837 The lower line shows positions of genes around this region (JGI Phytozome v 13,
838 *Chlamydomonas* database v 5.6 https://phytozome-next.jgi.doe.gov/). Numbers 19-559,
839 190065, and 9-0003 represent primer sets used for PCR. FAP16, FAP108, and FAP224
840 are genes of flagellar associated proteins (Pazour et al., 2005), FBB15 is a flagella/basal
841 body protein gene (Li et al., 2004), and TTLL2 is a putative tubulin tyrosine ligase gene
842 (Cre06.g300250, JGI Phytozome v 13, *Chlamydomonas* database v 5.6,
843 https://phytozome-next.jgi.doe.gov/). (D) The positions of the *bld13-1* and *bld13- 2*
844 mutations in the γ-tubulin amino acid sequence of *Chlamydomonas* and corresponding
845 sequences in other organisms. GenBank accession numbers are as follows: *C. reinhardtii*,
846 AAA82610.1; *A. nidulans*, CAA33507.1; *T. brucei*, XP_843687.1; *A. thaliana*, NP_191724.1;
847 *H. sapiens*, NP_001061.2; *M. musculus*, NP_598785.1; *D. melanogaster*, NP_476804.1; *S.*
848 *pombe*, NP_596147.1; *T. thermophila*, AAB65830.1; *C. elegans*, NP_499131.1; *E.*
849 *histolytica*, AAC08441.1.

850

851 **Fig. 2**.

852 Evidence supporting dominant-negative effects of the *bld13* mutations on ciliary
853 assembly. (A) Percentages of cells with zero, one, or two cilia in strains ectopically
854 expressing HA-tagged γ-tubulin from genomic fragments under the control of the
855 endogenous γ-tubulin promoter. These strains include a wild type strain expressing an
856 HA-tagged γ-tubulin (WT::γ-tub(WT)-HA), a wild type strain expressing the *bld13-1* γ-
857 tubulin (WT::γ-tub(T292I)-HA), a wild type strain expressing the *bld13-2* γ-tubulin
858 (WT::γ-tub(E89D)-HA), a *bld13-1* strain expressing the HA-tagged γ-tubulin (*bld13-1*::γ-
859 tub(WT)-HA), and a *bld13-2* strain expressing the HA-tagged γ-tubulin (*bld13-2*::γ-
860 tub(WT)-HA). Statistical analysis was performed using Fisher's exact test (***P < 0.001
861 for WT::γ-tub(WT)-HA vs *bld13-1*::γ-tub(WT)-HA, *bld13-2*::γ-tub(WT)-HA, and WT::γ-
862 tub(T292I)-HA; **P = 0.0013 for WT::γ-tub(WT)-HA vs WT::γ-tub(E89D)-HA; n>1500).
863 (B) Western blot analyses of whole cell lysates (10 μg/lane) of the wild type (WT),
864 *bld13-1*, *bld13-2*, WT::γ-tub(WT)-HA, WT::γ-tub(T292I)-HA, WT::γ-tub(E89D)-HA,
865 *bld13-1*::γ-tub(WT)-HA, and *bld13-2*::γ-tub(WT)-HA cells. The upper panel shows
866 immunoblotting with an anti-HA antibody detecting γ-tubulin(WT)-HA (55 kDa;
867 arrowhead), and the lower panel shows Coomassie Brilliant Blue (CBB) staining as a
868 loading control. (C) Percentages of cells with zero, one, or two cilia in diploid strains of
869 the wild type (WT/WT), heterozygous *bld13-1* (WT/*bld13-1*), heterozygous *bld13-2*
870 (WT/*bld13-2*), and *bld13-1*/*bld13-2*. Statistical analysis was performed using Fisher's
871 exact test (***P < 0.001 for WT/WT vs each mutant genotype and for WT/*bld13-2* vs
872 *bld13-1*/*bld13-2*; **P = 0.0036 for WT/*bld13-1* vs *bld13-1*/*bld13-2*; n >1500).
873
874 **Fig. 3.**
875 Localization of γ-tubulin in the presence or absence of *bld13* mutations. (A) Schematic
876 diagram showing microtubule organization and centriole positioning in the
877 *Chlamydomonas* cell. (B) Immunofluorescence images of WT::γ-tub(WT)-HA, *bld13-1*::γ-

878 tub(WT)-HA, *bld13-2*::γ-tub(WT)-HA, WT::γ-tub(T292I)-HA, and WT::γ-tub(E89D)-HA
879 cells stained with anti-HA (HA, green), anti-SAS-6 (SAS-6, magenta), and anti-acetylated
880 tubulin (Ac-tub, cyan) antibodies. Merged images show HA and SAS-6 signals (HA/SAS-
881 6) or SAS-6 and acetylated tubulin signals (SAS-6/Ac-tub). Scale bar: 500 nm. Filled
882 arrowheads indicate procentrioles, and open arrowheads indicate mature centrioles.
883 Representative images are shown; similar localization patterns were consistently
884 observed.
885
886 **Fig. 4.**
887 Effects of *bld13* mutations on microtubule organization in *Chlamydomonas* cells. All
888 images are shown as Z-projection images of confocal optical sections. (A)
889 Immunofluorescence images of wild-type, *bld13-1*, and *bld13-2* cells stained with anti-
890 acetylated α-tubulin antibody, which recognizes rootlet, axonemal, and centriolar
891 microtubules, but not non-rootlet cytoplasmic microtubules (Holmes and Dutcher,
892 1989). Cells were classified into four categories based on acetylated microtubule
893 organization: cells with three or fewer acetylated microtubules (≤3 MT), cells with four
894 rootlets (4 MT), cells with five or more acetylated microtubules (≥5 MT), and cells
895 lacking an obvious microtubule-organizing center but exhibiting a cage-like acetylated
896 microtubule (cage-like, CL). Representative images of each category are shown.
897 Arrowheads indicate rootlet or acetylated microtubules with unclear rootlet identity.
898 The graph shows the frequency of each category. (B) Immunofluorescence images of
899 wild-type, *bld13-1*, and *bld13-2* cells stained with an anti–α-tubulin antibody, which
900 labels non-rootlet cytoplasmic microtubules in addition to rootlet, axonemal, and
901 centriolar microtubules. Cells were classified using the same criteria as in (A), and the
902 frequency of each category is shown in the graph. Statistical analysis was performed
903 using Fisher's exact test (***$P < 0.001$; ns, not significant; $n>120$). Scale bars: 2 μm.

904

905 **Fig. 5.**

906 Partial loss of protofilaments in *bld13* centriolar triplet microtubules. (A) Electron
907 microscopic images of longitudinal and cross sections of centrioles in WT, *bld13-1*,
908 and *bld13-2* cells. Scale bars: 100 nm. (B) Magnified views of cross-sections of the triplet
909 microtubules in WT, *bld13-1*, and *bld13-2* centrioles. Asterisks indicate the positions of
910 protofilament loss. Scale bar: 40 nm. (C) Distributions of the protofilament loss in A- and
911 C-tubules of *bld13-1* and *bld13-2* triplet microtubules. A cross-sectional image of the A-
912 or C-tubule was divided into 12 or 6 sectors as shown in schematic diagrams (left, see
913 Materials and Methods). MIPs (in the lumen of the A-tubule), the A-C linker, and the
914 cartwheel spokehead, are drawn in grey (Li et al., 2019). The length of each bar in the
915 polar histograms (right) represents the relative frequency of protofilament loss at the
916 corresponding sector, expressed as a percentage of the total number of observed triplet
917 microtubule images. The x-axis of each graph is shown in 5% increments. Statistical
918 analysis was performed using the Hodges–Ajne test, showing that all distributions of the
919 protofilament loss are significantly non-uniform: *bld13-1* A-tubule ($P < 0.0001$; median:
920 sector 11), *bld13-2* A-tubule ($P < 0.0001$; median: sector 11), *bld13-1* C-tubule ($P <$
921 0.0001; median: sector 4), *bld13-2* C-tubule ($P < 0.0001$; median: sector 4).

922

923 **Fig. S1.**

924 Effects of the *bld13* mutations on the γ-tubulin structure predicted by AlphaFold2. (A)
925 AlphaFold2 models of the *bld13-1* and *bld13-2* γ-tubulin molecules (blue) are merged
926 with that of the wild-type (green). The mutation sites (T292I and E89D) are shown in
927 white. (B) An amino acid sequence alignment of human γ-tubulin (Acc. No.
928 NP_001061.2) and *Chlamydomonas* γ-tubulin (Acc. No. AAA82610.1). Amino acids
929 homologous or conserved between the two proteins were identified by Clustal Omega

930 (Sievers and Higgins, 2014) and indicated by an asterisk or dot, respectively. Indicated
931 by color are the amino acids located on the + end surface (green) and the - end surface
932 (light blue), and those close to the adjacent γ-tubulin molecules (blue and pink). The
933 positions of the mutated amino acids (E86 and T292) are indicated with yellow and red
934 boxes. Note that they are one of the amino acids located close to the adjacent γ-tubulin.
935 (C) Positions of the amino acid changes on the γ-tubulin 3-D structure. A model of the
936 human γ-tubulin 3-D structure, based on the PDB file 1Z5W (Aldaz et al., 2005), is
937 generated using PyMOL (right). This model shows the surface of the γ-tubulin molecule
938 in the same orientation as in the γ-TuRC (left). The colors correspond to those in (B).
939

940 Figures

Figure 1

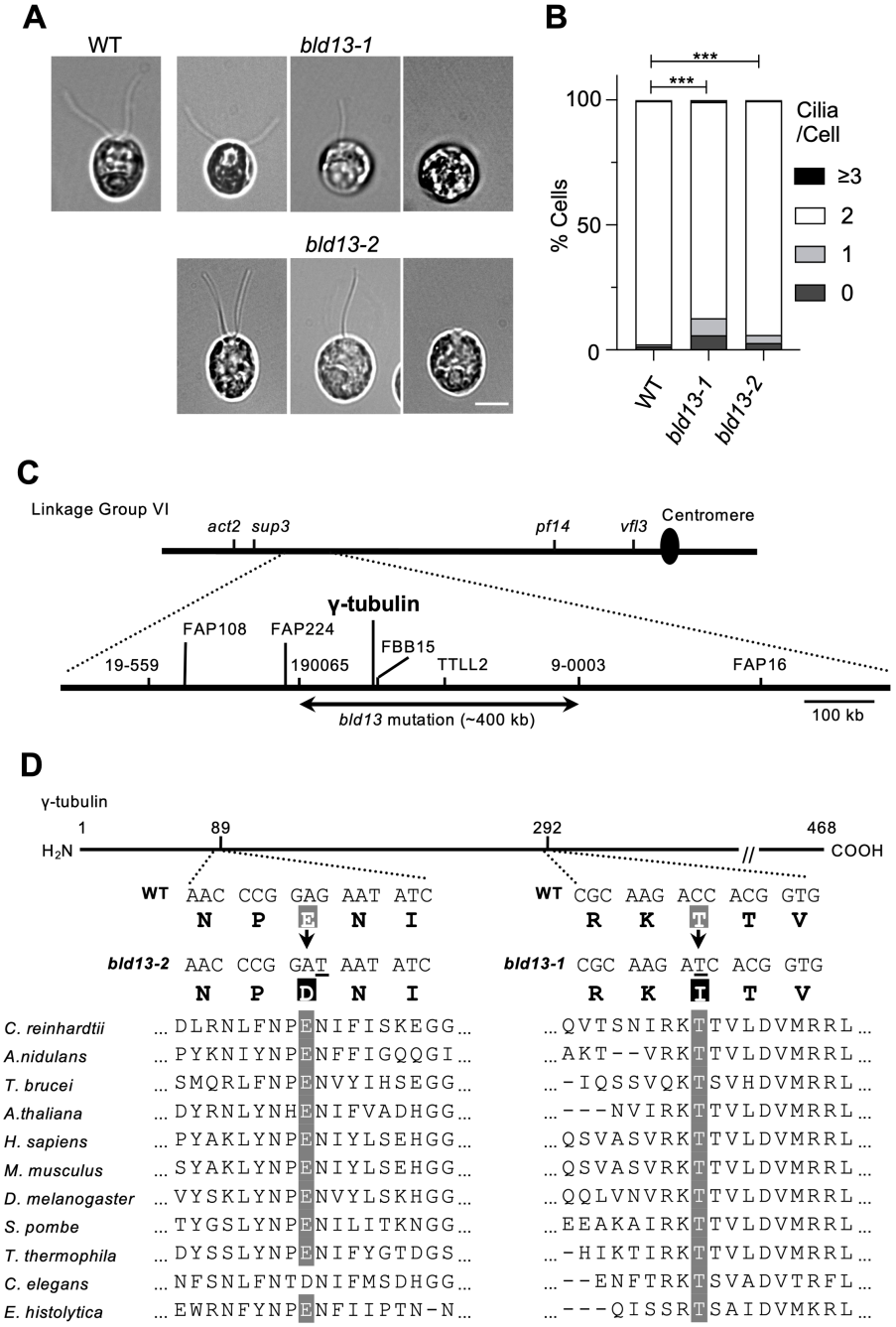

941

Figure 2

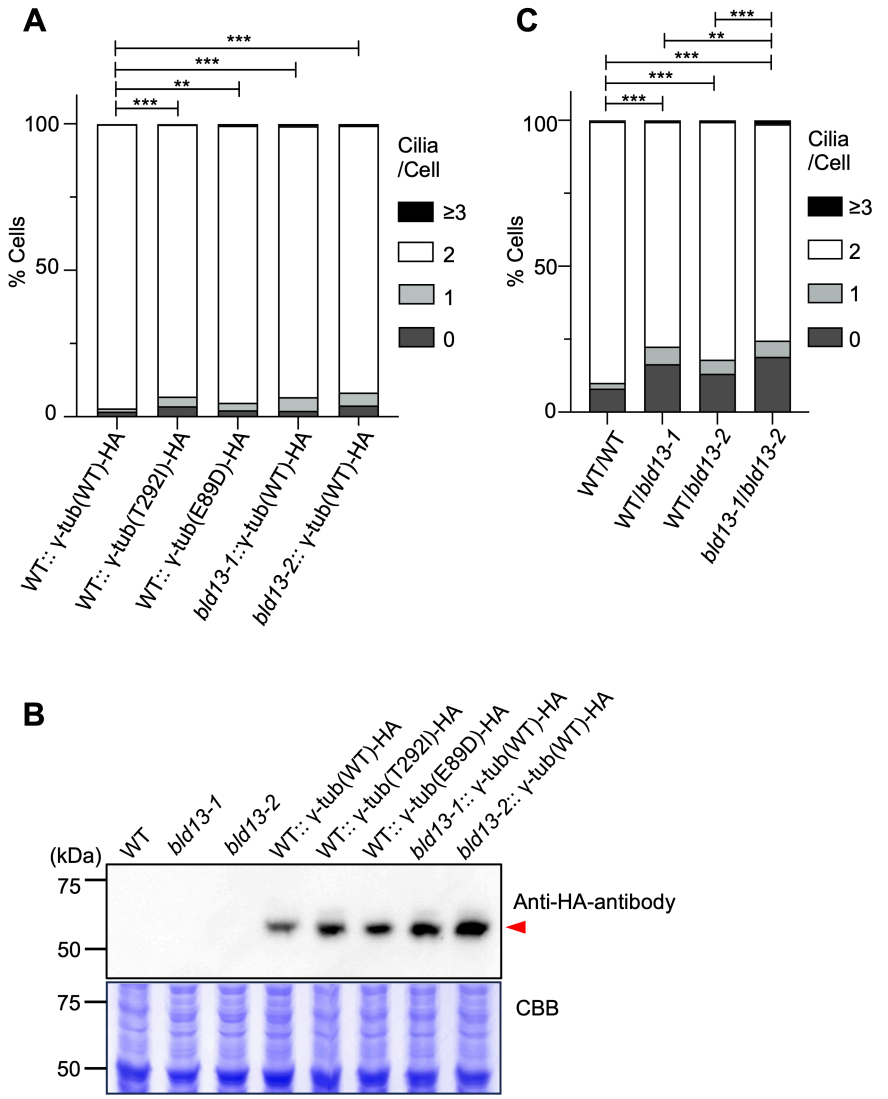
A
***
***
**
***
100
50
0
% Cells
Cilia
/Cell
≥3
2
1
0
WT:: γ-tub(WT)-HA
WT:: γ-tub(T292I)-HA
WT:: γ-tub(E89D)-HA
bld13-1::γ-tub(WT)-HA
bld13-2:: γ-tub(WT)-HA
C
***
**
***
***
***
100
50
0
% Cells
Cilia
/Cell
≥3
2
1
0
WT/WT
WT/bld13-1
WT/bld13-2
bld13-1/bld13-2
B
WT
bld13-1
bld13-2
WT:: γ-tub(WT)-HA
WT:: γ-tub(T292I)-HA
WT:: γ-tub(E89D)-HA
bld13-1:: γ-tub(WT)-HA
bld13-2:: γ-tub(WT)-HA
(kDa)
75
50
Anti-HA-antibody
75
50
CBB

942

Figure 3

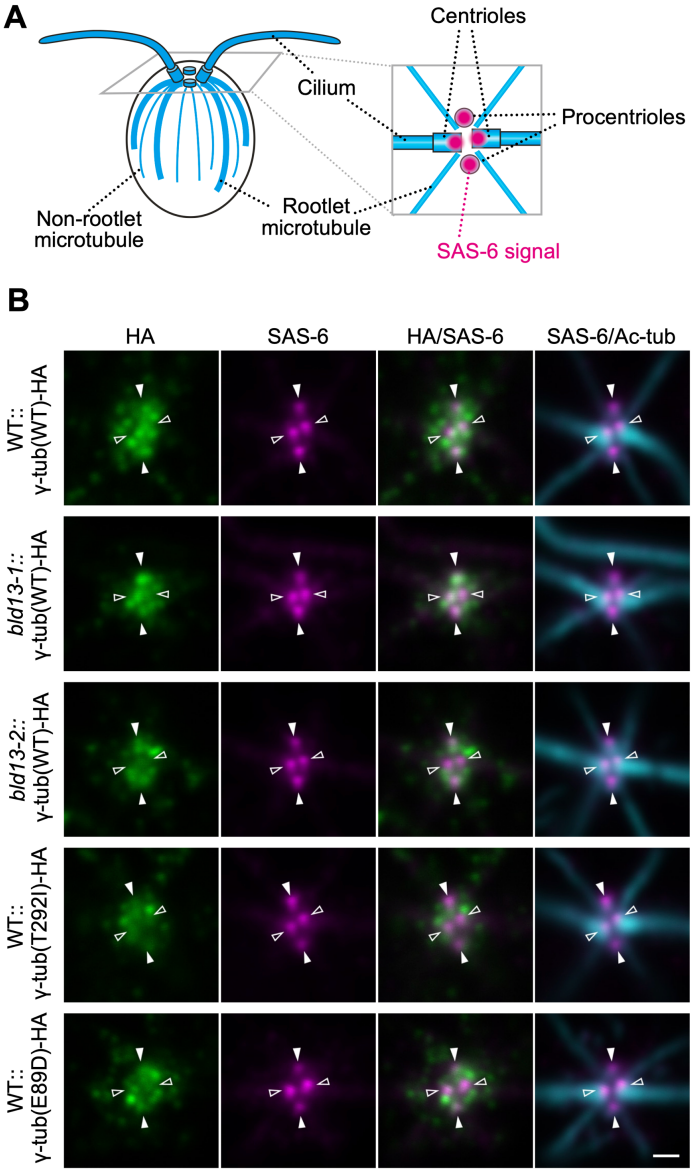
A
Centrioles
Cilium
Procentrioles
Non-rootlet microtubule
Rootlet microtubule
SAS-6 signal
B
HA
SAS-6
HA/SAS-6
SAS-6/Ac-tub
WT::γ-tub(WT)-HA
bld13-1::γ-tub(WT)-HA
bld13-2::γ-tub(WT)-HA
WT::γ-tub(T292I)-HA
WT::γ-tub(E89D)-HA

943

944

Figure 4

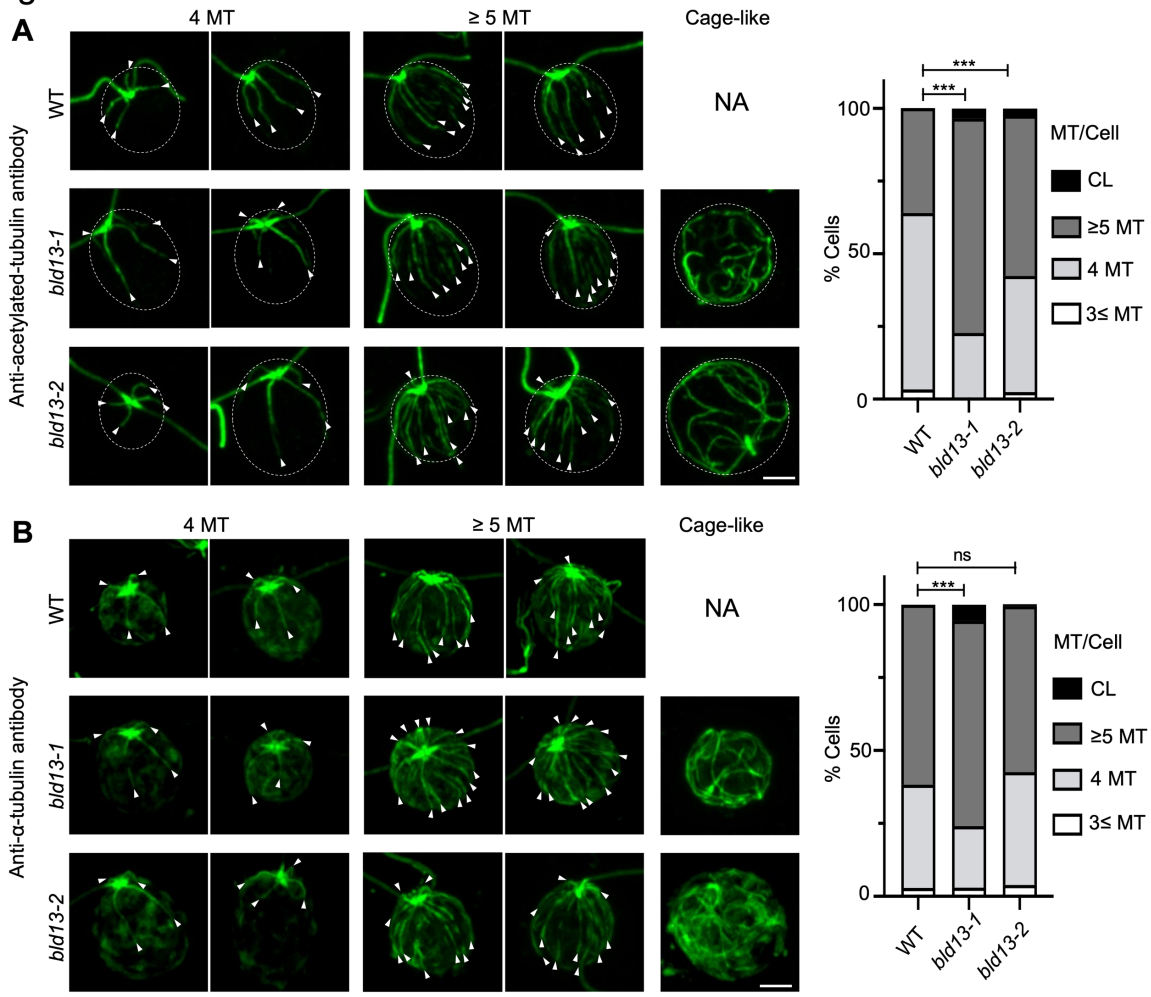
A
4 MT
≥ 5 MT
Cage-like
Anti-acetylated-tubulin antibody
WT
bld13-1
bld13-2
NA
***
***
100
50
0
% Cells
MT/Cell
CL
≥5 MT
4 MT
3≤ MT
WT
bld13-1
bld13-2
B
4 MT
≥ 5 MT
Cage-like
Anti-α-tubulin antibody
WT
bld13-1
bld13-2
NA
ns
***
100
50
0
% Cells
MT/Cell
CL
≥5 MT
4 MT
3≤ MT
WT
bld13-1
bld13-2

Figure 5

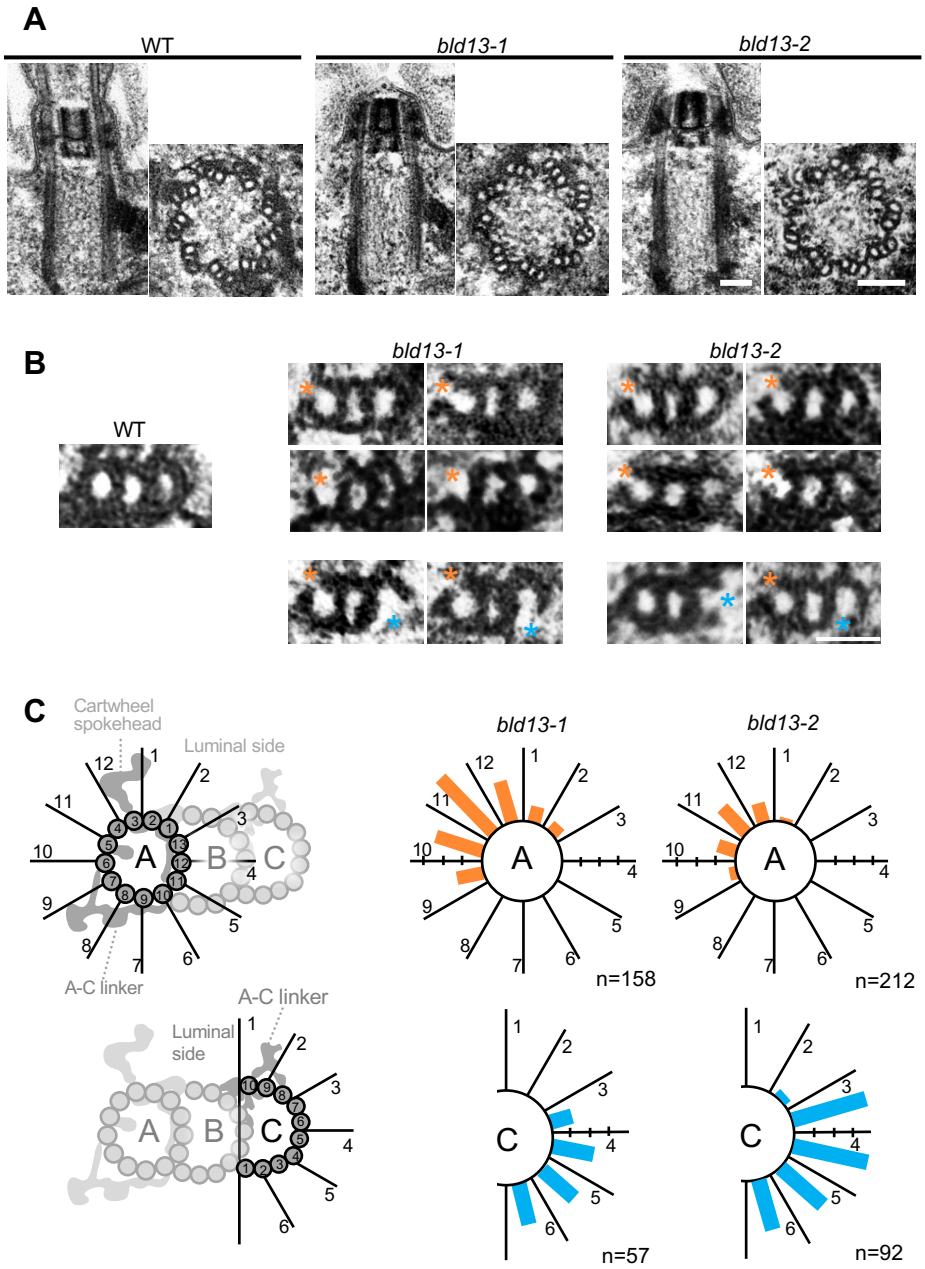
A
WT
bld13-1
bld13-2
B
WT
bld13-1
bld13-2
C
Cartwheel spokehead
Luminal side
A-C linker
A
B
C
bld13-1
bld13-2
n=158
n=212
n=57
n=92

945

Figure S1

A

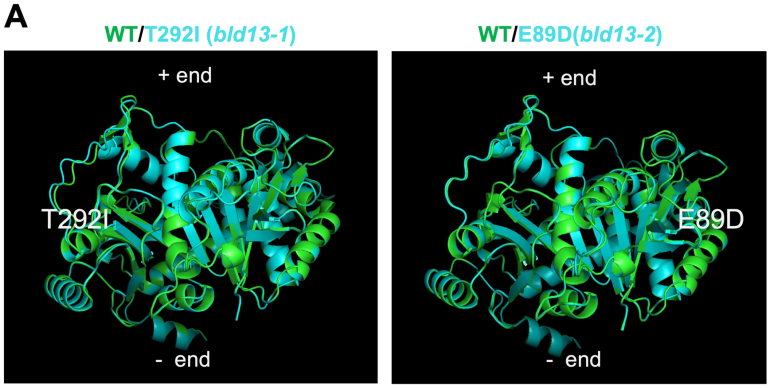

B

```
Cre     MPREIINLQVGQCGNQVGSEFWRKLCQEHGIAKDGRLEDFATLGGDRKDVFFYQADDEQY     60
Hsa     MPREIITLQLGQCGNQIGFEFWKQLCAEHGISPEGIVEEFATEGTDRKDVFFYQADDEHY     60
        ******.**:******:* ***::** ****: :* :*:*** * **************:*

Cre     IPRAILLDLEPRVINGIQTSDLRNLFNPENIFISKEGGGAGNNWASGYTQGEAVQETLLD     120
Hsa     IPRAVLLDLEPRVIHSILNSPYAKLYNPENIYLSEHGGGAGNNWASGFSQGEKIHEDIFD     120
        ****:*********:.* .*   :*:*****::*:.***********::*** ::* ::*

Cre     MIDREAEYCDSLEGFNMCHSIAGGTGSGMGSYMLELISDRYSKKLIQTYSVFPNQSESSD     180
Hsa     IIDREADGSDSLEGFVLCHSIAGGTGSGLGSYLLERLNDRYPKKLVQTYSVFPNQDEMSD     180
        :*****: .****** :***********:***:** :.*** ***:*********.* **

Cre     VVVQPYNSLLTLKRLTLHADAVVVLDNTALDKIAVERLHLHKPDVQQINSLIATVMAAST     240
Hsa     VVVQPYNSLLTLKRLTQNADCVVVLDNTALNRIATDRLHIQNPSFSQINQLVSTIMSAST     240
        **************** :**.*********::**.:***:::*...***.*::*:*:***

Cre     TTLRYPGYMNNDLVGLVASLIPTPRCHFLMTGYTPLTAENAAGQVTSNIRRTFVLDVMRR     300
Hsa     TTLRYPGYMNNDLIGLIASLIPTPRLHFLMTGYTPLTTDQS----VASVRRTFVLDVMRR     296
        *************:**:******** ***********::::    .:.:***********

Cre     LLQPKNIMVSTHTKSRDIANAKYISILNIIQGEVDPSQVHKSLQRIRERKQANFIEWGPA     360
Hsa     LLQPKNVMVSTGRD--RQTNHCYIAILNIIQGEVDPTQVHKSLQRIRERKLANFIPWGPA     354
        ******:****  .    :*  **:***********:************* **** ****

Cre     SIQVALSKKSPYVQTAHRVSGLMLANHTSVRHLFNKVLRDYEKLMGPKQERQAFMQAYRD     420
Hsa     SIQVALSRKSPYLPSAHRVSGLMMANHTSISSLFERTCRQYDKLRK----REAFLEQFRK     410
        *******:****: :********:*****:  **::. *:*:**      *:**:: :*.

Cre     VPRFADAAGGGTALLEEFADAKEVVQDLANEYAACESADYIQRQMMAS    468
Hsa     EDMFKDN-------FDEMDTSREIVQQLIDEYHAATRPDYISWGTQEQ    451
           * *        ::*:  ::*:**:* :** *.   ***.     .
```

C

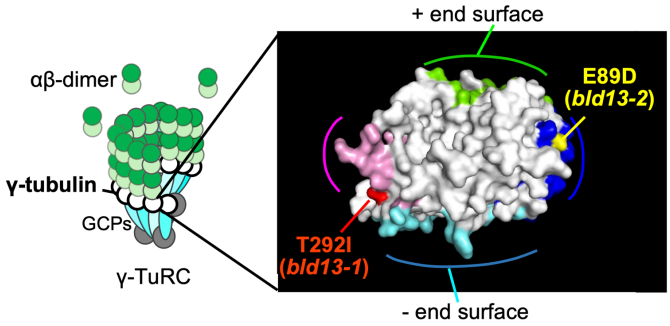

946